Air-sea CO₂ fluxes in the near-shore and intertidal zones influenced by the California Current

Janet J. Reimer,[1,2] Rodrigo Vargas,[2,3] Stephen V. Smith,[4] Ruben Lara-Lara,[5] Gilberto Gaxiola-Castro,[5] J. Martín Hernández-Ayón,[6] Angel Castro,[2,7] Martin Escoto-Rodriguez,[2] and Juan Martínez-Osuna[2]

[1] The study of air-sea CO_2 fluxes (FCO_2) in the coastal region is needed to better understand the processes that influence the direction and magnitude of FCO_2 and to constrain the global carbon budget. We implemented a 1 year (January through December 2009) paired study to measure FCO_2 in the intertidal zone (the coastline to 1.6 km offshore) and the near-shore (~3 km offshore) off the north-western coast of Baja California (Mexico); a region influenced by year-round upwelling. FCO_2 was determined in the intertidal zone via eddy covariance; while in the near-shore using mooring buoy sensors then calculated with the bulk method. The near-shore region was a weak annual net source of CO_2 to the atmosphere (0.043 mol CO_2 m^{-2} y^{-1}); where 91% of the outgassed FCO_2 was contributed during the upwelling season. Sea surface temperature (SST) and ΔpCO_2 (from upwelling) showed the strongest relationship with FCO_2 in the near-shore, suggesting the importance of meso-scale processes (upwelling). FCO_2 in the intertidal zone were up to four orders of magnitude higher than FCO_2 in the near-shore. Wind speed showed the strongest relationship with FCO_2 in the intertidal zone, suggesting the relevance of micro-scale processes. Results show that there are substantial spatial and temporal differences in FCO_2 between the near-shore and intertidal zone; likely a result of heterogeneity. We suggest that detailed spatial and temporal measurements are needed across the coastal oceans and continental margins to better understand the mechanisms which control FCO_2, as well as reduce uncertainties and constrain regional and global ocean carbon balances.

1. Introduction

[2] The coastal ocean along continental margins is an important environment in terms of the uptake of CO_2 as this region is responsible for approximately 15% to 30% of oceanic primary production [*Gattuso et al.*, 1999]; yet estimates of net global air-sea CO_2 fluxes (FCO_2) in the coastal ocean are largely uncertain as there is a wide range of values reported in the literature and for the various coastal ocean processes involved [*Borges et al.*, 2005; *Laruelle et al.*, 2010]. Therefore, it is necessary to better understand the ocean carbon cycle and, more specifically, the air-sea exchange of CO_2 along the continental margins [*Alin et al.*, 2012], which are ecologically and socially important [*Vargas et al.*, 2012].

[3] A variety of methods are used to determine the FCO_2, including both direct and indirect methods. FCO_2 has been directly measured using shipboard and stationary eddy covariance (EC) as well as bulk calculation methods based on the air-sea differential. Other methods have calculated FCO_2 across ocean basins using climatological data [*Takahashi et al.*, 2002, 2009]. Unfortunately, the output of

these calculations fails to produce information along the global coastline due to limitations in the temporal and spatial distribution of data (i.e., wind fields and partial pressure of carbon dioxide (pCO$_2$)) of the surface ocean. Based on in situ FCO$_2$ measurements in the coastal ocean, indirect scaling calculations using the surface area of a particular region and reported FCO$_2$ have also been applied [*Frankignoulle and Borges*, 2001; *Borges*, 2005; *Borges et al.*, 2005; *Laruelle et al.*, 2010]. Scaling studies, though important as broad scale estimations, cannot capture important fine scale spatial differences which in situ studies of coastal FCO$_2$ have the ability to determine. The wide range in values of in situ coastal FCO$_2$ is likely to lead to even greater uncertainties in the global FCO$_2$ as there is the potential to under or over estimate FCO$_2$ when integrated over time and space [*Wollast*, 1991; *Takahashi et al.*, 2009; *Ribas-Ribas et al.*, 2011]. Therefore, understanding of the different biological and physical processes that control FCO$_2$ along the various coastal settings of continental margins is necessary in order to better constrain the global FCO$_2$.

[4] Over the last 2 decades, there has been a wide range of FCO$_2$ values reported for various near-shore, coastal, and inner shelf environments: -5.1 to 5.1 mol m^{-2} y^{-1} for continental shelves [*Bates*, 2006; *Friederich et al.*, 2008, respectively], and -3.9 to 76 mol m^{-2} y^{-1} for coastal embayments and estuaries [*Koné et al.*, 2009; *Frankignoulle et al.*, 1998, respectively]. This wide range of values has been attributed to the heterogeneity and coupled biogeochemical processes in near-shore and coastal systems [*Laurelle et al.*, 2010]. Due to present uncertainties, there is a critical need for the implementation of long-term, high-resolution (temporal and spatial) studies of CO$_2$ dynamics in the coastal region in order to reduce the various sources of uncertainty and constrain the range of FCO$_2$ values [*Borges et al.*, 2009; *Vargas et al.*, 2012].

[5] The region through which the California Current passes (from the Pacific Northwest of the United States to the southern tip of the Baja California peninsula) is important in terms of the various fisheries, including shellfish [*Barton et al.*, 2012], sardines, and anchovies [*Chavez et al.*, 2003], which depend on the high rates of phytoplankton production in the upwelling regime [*Palacios et al.*, 2004]. It is important to understand the CO$_2$ dynamics in this region due to its biological and economic relevance, yet the available literature present varying magnitudes and/or direction for FCO$_2$. For example, for the region between $30°$ to $60°$N synthesis studies have concluded that the region is a weak sink for CO$_2$: -0.11 and -1.0 mol m^{-2} y^{-1} [*Borges et al.*, 2005; *Cai et al.*, 2006, respectively], while *Laurelle et al.* [2010], using a slightly higher shelf area (0.06×10^6 km^2) than two former studies, estimated 3.2 mol m^{-2} y^{-1} (a net source of CO$_2$). The California Cooperative Fisheries Investigations (CalCOFI) line 67 in front of Monterey Bay has been reported to be both a net annual source and sink for CO$_2$: from July 1997 to July 1998 (El Niño) -0.30 mol m^{-2} y^{-1} and 2.2 mol m^{-2} y^{-1} for the following 12 month La Niña period [*Friederich et al.*, 2002]. According to the previous in situ and synthesis-based studies, the direction of the flow of CO$_2$ for the region depends on the study location and/or El Niño Southern Oscillation mode (i.e., synoptic-scale climatic conditions). The area between $30°$N to $60°$N is quite large; within this region there are many spatial differences, including locally specific river outflows with estuarine conditions, arid climates, wave size, and upwelling strength; in other words, variability due to different biological and physical processes. There is a need to first understand the magnitudes and location of these differences and then the processes which drive these differences.

[6] The objective of this study was to determine the temporal patterns and magnitudes of FCO$_2$ in an upwelling region in the intertidal zone and near-shore waters influenced by the California Current. We established a paired study and evaluated how wind speed (physical forcing for water column turbulence) and sea surface temperature (SST; as an indicator of upwelling as well as for gas solubility) influenced the temporal pattern and magnitude of FCO$_2$ in the two zones during one calendar year. We implemented the paired study to show the importance of obtaining data from distinct ocean environments within close proximity, which exhibit both similar and dissimilar water column conditions (depending on the season) with the same atmospheric conditions, and yet different FCO$_2$ values. Our combined experimental approach was based on high frequency measurements (1 to 3 hour resolution) and lower frequency measurements (daily averages (24 hour resolution)). First, we studied the magnitude (daily and hourly) of FCO$_2$ in the region in front of Ensenada, Baja California, Mexico. Second, we focused on three specific times of the year (i.e., case studies: upwelling, relaxed conditions, and the onset of an upwelling event) to investigate the relevance of high- (changes in wind speed) and low-frequency (changes in SST and the air-sea gradient of pCO$_2$ (i.e., ΔpCO$_2$)) controls on the dynamics of FCO$_2$ in two environments: the near-shore and intertidal zone. We show that even when it appears that biological and chemical properties of the water column are similar, it is the different physical processes that drive the direction and magnitude of FCO$_2$ between the intertidal zone and near-shore waters.

2. Methods

2.1. Study Site

[7] For the purposes of this work, we define the "intertidal zone" as the area that a stationary eddy covariance (EC) tower was measuring: because the measurement of FCO$_2$ using EC is sensitive to the direction and speed of the wind, the footprint (i.e., the area with high probability of being measured) is always changing; therefore, the dimensions of this region are not fixed but varied over the course of the study. Depending on the wind speed, the footprint for this study typically ranged from approximately 500 to 900 m but reached up to 1.6 km with the strongest winds (≥ 12 m s^{-1}). The method of *Schuepp et al.* [1990] was used to calculate the footprint. During the study, even with the dynamic footprint, the intertidal zone was always composed of the both the neritic zone (supralittoral, littoral and sublittoral regions) and the oceanic zones (extending over the continental slope). We define the "near-shore" as the region where the buoy was measuring: the oceanic region 3 km off the coast (this site is located at a distance greater than that of the footprint from the EC tower), characterized by deeper waters (>90 m) than the intertidal zone, and is located over the continental slope (Figure 1).
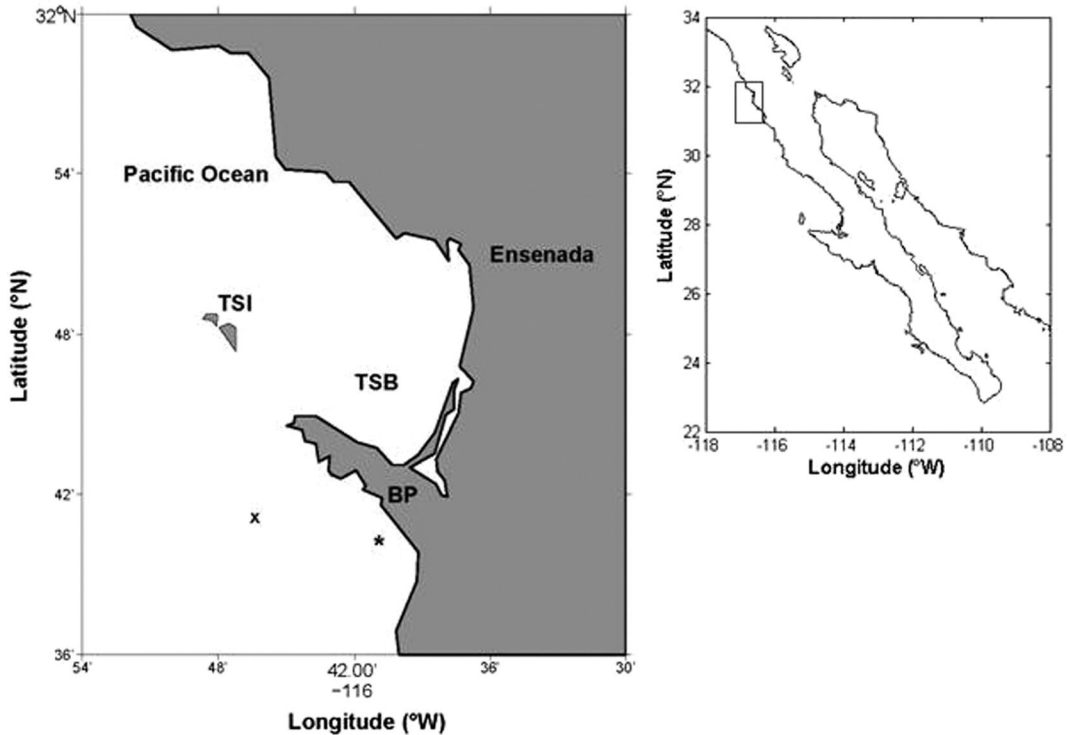
Figure 1. Map of the study region outside of Todos Santos Bay (TSB) showing the location of the EC tower (northwestern tip of Todos Santos Island [TSI]) in the intertidal zone and the buoy (star) in the near-shore off of Banda Point (BP). The "x" shows the location of IMECOCAL station 100.30 (salinity and water column temperature data). Insert shows the location of Todos Santo Bay (square) on the Baja California Peninsula.

[8] It should be noted that the Pacific coast off Baja California lies in a region where upwelling occurs year round [*Bakun*, 1975], but that the spring and summer months (March to August) typically present the strongest and most sustained upwelling with the lowest SSTs [*Feely et al.*, 2008]. The paired study was carried out during 2009 and consisted of FCO_2 measurements from the two discrete sites just outside of Todos Santos Bay near Ensenada, Mexico (Figure 1).

[9] Due to physical differences in the location of the sites, different techniques were used to measure FCO_2. Measurements of FCO_2 and wind were recorded at the EC tower was located on Todos Santos Island (31.81056°N, 116.80889°W) approximately 19 km off the coast of Ensenada. The EC tower was physically located in the supralittoral zone on the windward side of Todos Santos Island, slightly landward of mean high water (sensors at 23.6 m above sea level: this height is that of the tower plus the elevation of the land surface above sea level). The surf zone in front of the EC tower is characterized by rocky outcroppings and a narrow (2–3 m) rocky beach at low tide, otherwise at high tide the waves break on the natural rocky outcroppings. This site was chosen to be on an island due to the fact that it is offshore away from potential anthropogenic influences yet still in the coastal upwelling region and in a high surf zone. We also collected data from a mooring buoy, which consisted of CO_2, SST, and salinity sensors (as well as other sensors not part of the present study) located approximately 3 km off the coast of Banda Point (31.66694°N, 116.68500°W; Figure 1).

2.2. Data Collection and Analysis: Eddy Covariance Tower

[10] First, we calculated FCO_2 in the intertidal zone using an EC tower equipped with an infrared gas analyzer (LI-7500, LICOR, Lincoln, NE, USA) and a sonic anemometer (Young 8100, Traverse City, MI, USA) with variables measured at 20 Hz. The infrared gas analyzer sensors were calibrated using an ultra pure CO_2 gas standard every 3–4 weeks. The manufacturer determined precision of the instrument was 0.11 µmol mol^{-1} CO_2. Initially, half-hour averages of FCO_2 (i.e., high frequency data: µmol m^{-2} s^{-1}) for this region were determined using the EC method, which has become the primary method used to study terrestrial FCO_2 [*Baldocchi et al.*, 2001]; and has also been used in coastal [*Lueker et al.*, 2003; *Riley et al.*, 2005] and open ocean environments [*McGillis et al.*, 2001; *Grachev et al.*, 2011]. The general EC equation is

$$FCO_2 = \overline{\rho_a w' s'} \qquad (1)$$

where FCO_2 is the CO_2 flux, ρ_a is the mean air density, w' is the vertical wind speed, and s' is the mixing ratio of CO_2; the prime indicates that these values are the fluctuations about their respective means and the overbar indicates covariance of FCO_2 in passing air masses. *Wanninkhof et al.* [2009] point out that the EC method is not only the "purest" measurement for FCO_2, but that it is best suited for regions with high magnitude sources/sinks of CO_2, such as coastal and/or upwelling regions. From the initial

half-hour values, we calculated the high frequency (i.e., 1 h averages: µmol m^{-2} s^{-1}) and low frequency measurements (i.e., daily averages: mol m^{-2} d^{-1}). Daily averages were calculated in order to observe the annual time series (year 2009). When the half-hour averages were determined, quality control/quality assurance procedures were applied for FCO$_2$ calculations; these include: de-spiking [*Vickers and Mahrt*, 1997], de-trending [*Moncrieff et al.*, 2004], temperature and water vapor fluctuation (Webb-Pearman-Leuning) correction [*Leuning*, 2007], and sonic corrections [*Schontanus et al.*, 1983]. The average wave height (data obtained from the daily average wave height model available at http://www.previmer.org) was used as the roughness height (i.e., the height above a surface of the roughness sublayer that creates a turbulent flow) for the application of the post processing corrections for FCO$_2$ in the intertidal zone.

[11] In order to analyze only marine-derived FCO$_2$ from the EC tower, we excluded FCO$_2$ associated to winds from the directions of the island and mainland (from the northeast, east, and southeast: ≤150 and ≥330 degrees) prior to the calculation of 1 h averages. It should be mentioned that winds from the northwest typically induce upwelling along the coast in this particular region [*Bakun*, 1975]. Prior to the calculation of the 1 h FCO$_2$ averages and the application of the wind direction filter, we also eliminated FCO$_2$ outliers (arbitrarily chosen as ± 3 standard deviations) which were <−61 and >61 µmol m^{-2} s^{-1}. It is assumed that since FCO$_2$ associated to wind directions from the island and mainland were eliminated, there are no local anthropogenic emissions included in the dataset. There is a large gap in the data between the 107th day of the year through the 230th due to instrument failure. The present dataset allows us to analyze the dynamics of FCO$_2$ under different conditions (upwelling and nonupwelling) because upwelling in this region occurs year round, although typically more sporadically during the "non-upwelling season," generally from September through February [*Bakun*, 1975].

2.3. Data Collection and Analysis: Mooring Buoy at Station Ensenada

[12] Second, we measured pCO$_2$ of the air 1 m above sea level and pCO$_2$ just below the surface as well as SST at 3 h intervals using the buoy-mounted sensors at Station Ensenada: 31.66694°N, 116.68500°W [*Linacre et al.*, 2010]. The pCO$_2$ system was designed and constructed at the Monterey Bay Aquarium Research Institute. The mooring system is described in detail in *Friederich et al.* [1995] and *Friederich et al.* [2002]; instrument uncertainty was <1 ppm, with calibration errors accounting for <1% of the value of the measurements. This instrumentation autocalibrates in situ using air. Then when the data are processed, this calibration is factored into the calculations for pCO$_2$. The performance of the sensor is revised approximately every 2 months.

[13] We calculated FCO$_2$ in the near-shore using the widely accepted bulk air-sea CO$_2$ equation. FCO$_2$ (µmol m^{-2} s^{-1}) was determined at 3 h intervals and were then used to calculate daily averages (mol m^{-2} d^{-1}) and the annual net FCO$_2$ (mol m^{-2} y^{-1}). FCO$_2$ from the buoy was calculated using the bulk equation with a transfer velocity

based on the cubic wind speed relationship [*Wanninkhof and McGillis*, 1999]

$$F\mathrm{CO}_2 = ks\Delta p\mathrm{CO}_2 \qquad (2)$$

where FCO$_2$ is the air-sea CO$_2$ flux, ΔpCO$_2$ is the difference between the partial pressure of CO$_2$ in the surface water and the air 1 m above sea level, k is the gas transfer velocity (cubic wind speed), and s is the solubility coefficient. The transfer velocity was calculated using various Schimdt numbers (assuming a smooth surface regime) normalized to 600 in accordance with *Wanninkhof and McGillis* [1999]. The bulk equation with a k calculated using the cubic wind speed relationship has been repeatedly chosen to use at study sites with stronger and/ or more persistent winds [*De La Cruz-Orozco et al.*, 2010; *Edson et al.*, 2011; *Ribas-Ribas et al.*, 2011; *Vandemark et al.*, 2011]. An analysis of the different formulations of the bulk calculation [including *Wanninkhof and McGillis*, 1999; *Ho et al.*, 2006; *Nightingale et al.*, 2000] was carried out to determine the differences in the value of FCO$_2$; the results showed that both the *Ho et al.* [2006] and *Nightingale et al.* [2000] calculations gave much higher (by up to 97%) results than data derived using the *Wanninkhof and McGillis* [1999] formulation (data not shown). *Edson et al.* [2011] suggest that at wind speeds up to 18 m s^{-1}, the cubic relationship offers a good representation of bubble-mediated gas transfer; in the present study, wind speeds reached up to about 15 m s^{-1}. Most importantly, the *Wanninkhof and McGillis* [1999] formulation was calibrated using data obtained via the EC method. This may reduce the variability in the data between the two sites as well as due to the use of the two methods; this is based on the assumption that this formulation will pick up all the features that the EC method would. Therefore, we believe that the *Wanninkhof and McGillis* [1999] formulation of the bulk equation is the best representation to use in the present study. We use the widely accepted convention that negative FCO$_2$ values represent transfer of CO$_2$ from the atmosphere into the ocean (uptake), and a positive value represents the release (outgassing) of CO$_2$ out of the ocean into the atmosphere for both methods (i.e., EC tower and buoy).

[14] Missing air pCO$_2$ data from the buoy due to sensor failure (approximately 44% of the data) was replaced by the air pCO$_2$ from the Globalview database [*Takahashi et al.*, 2002, 2009; *McNeil et al.*, 2007]; specifically from the Scripps Institute of Oceanography station (the La Jolla Pier). We identified good agreement between the Globalview and our buoy data sets based on linear regression analysis ($r^2 = 0.80$; $p > 0.001$; $n = 365$). Furthermore, the percent difference between in situ measurements and Global-view data ranged from −0.55% to 6.98% with an average difference of 1.40% ± 1.60%.

[15] FCO$_2$ from the buoy was calculated using wind data collected from a meteorological station located on Todos Santos Island. The meteorological station used for calculation of the buoy FCO$_2$ is located <1 km from the EC tower; we found a significant correlation between wind speed measurements at both stations ($r = 0.82$, $p < 0.001$). For all statistical analyses between the FCO$_2$ (from both
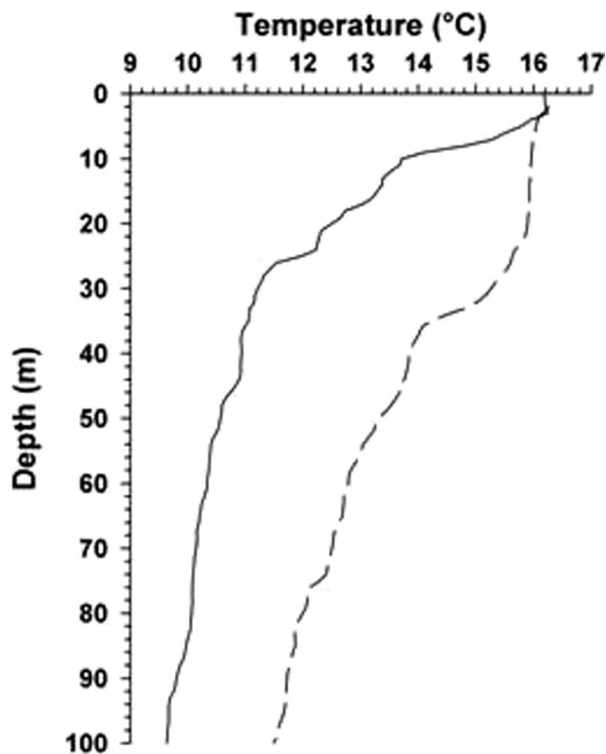
Figure 2. Temperature profiles for the water column at IMECOCAL station 100.30 outside of Todos Santos Bay. The solid line is the April 23, 2009 cruise and the dashed line is the October 30, 2009 cruise.

stations) and wind velocity, the wind data collected at the EC tower was used because it was recorded at a higher frequency than that of the meteorological station used to calculate FCO$_2$ at the mooring buoy.

[16] Water column temperature (Figure 2 and Figure S1, online only) and salinity data (Figure S2, online only) were collected during Investigaciones Mexicanas de la Corriente de California (IMECOCAL; part of the Mexican Carbon program [FLUCAR]; [see *Vargas et al.*, 2012]) cruises on April 23 and October 30, 2009 along IMECOCAL/Cal-COFI line 100 (see *Linacre et al.* [2010] for IMECOCAL transect information), which is in the same general region as our buoy (Station Ensenada). Level three (L3), 8-day, 4 km SeaWiFS chlorophyll *a* (Chla) data was obtained from the NASA Giovanni server (http://disc.sci.gsfc.nasa.gov/giovanni/overview/index.html). The time series of Chla is an average of data for the area of 31.4681°N to 31.8481°N and 116.8169°N to 116.6519°N. Due to the proximity of both sites to the coast (<4 km from a land mass), we chose one representative region in between both sites: the region between Todos Santos Island and the buoy outside of the mouth of Todos Santo Bay and more than 4 km off Todos Santos Island and the tip of Banda Point.

[17] For analysis between sites, first, half-hour data from the intertidal zone were averaged at 3 h intervals for appropriate comparisons (the sampling interval of the buoy was 3 hours while the EC tower fluxes were calculated as half-hour averages). Second, we used multiple linear regression (MLR) analysis to determine which variable (i.e., ΔpCO$_2$, SST, or wind speed) contributed most to the variability of

FCO$_2$ at each site for each of the case study time periods (see section 2.3). The MLR was chosen as we are not aware of a nonlinear equation that is commonly used to represent the complex interactions between biophysical and geochemical processes with FCO$_2$. Therefore, we were conservative and followed linear approaches due to the parsimony principle, as well as to avoid over-fitting the data by using a nonlinear approach, which may be potentially difficult to interpret. We recognize that the complexity of FCO$_2$ ocean processes are nonlinear and must be addressed as a priority research topic [*Bates and Merlivat*, 2001]. We interpret the remaining variability (i.e., residual values of the MLR) as variability likely due to an unmeasured variable or to nonlinear processes that are not captured by the empirical MLR approach. It should be pointed out that the overall biological component (i.e., photosynthesis/respiration and bacterial-mediated remineralization) is represented in the ΔpCO$_2$ measurements. We are unable to separate this term as we did not explicitly measure biological components associated with CO$_2$ fixation/production. The MLR was used to determine the importance of the different independent variables in predicting FCO$_2$ at the two selected locations across three case studies: upwelling, relaxed conditions, and the onset of an upwelling event.

[18] Third, we applied regression tree analysis, which uses recursive partitioning to predict nonlinear responses grouped into clusters [*Breiman et al.*, 1984]. This analysis serves as a visual representation of how the combination of the different factors analyzed (ΔpCO$_2$, SST, and wind speed) may be used to predict the FCO$_2$ at each site. We used a minimum node size of five, meaning that in each terminal point the predictive R^2 of the model is represented by at least five values. We applied this model to both the EC tower and buoy data combining all the data from the three case studies of different conditions, and used it as a comparison with the MLR approach.

[19] Fourth, FCO$_2$ data from both sites were compared with SST and wind speed using cross correlation analysis to determine the lags (if any) with FCO$_2$. This analysis was applied as a measure of similarity between two different measurements (time series) as a function of a time lag applied to one of them. We interpreted the results of this analysis as the delay (lags) between two measurements, which provides information on the nature and origin of coupling between the processes and causality under the assumption that the effect (FCO$_2$) must follow the cause (ΔpCO$_2$, SST, and wind speed). Specifically, one lag unit is equal to one 3 h period (the frequency of measurements) for this study. The data was analyzed based on the assumption that the FCO$_2$ was the dependent variable (the effect) and that ΔpCO$_2$, SST, or wind speed was the independent variable (the cause). Cross correlation results were determined for a $p < 0.05$. Similar analysis has been done to evaluate lags for CO$_2$ fluxes in terrestrial ecosystems [*Vargas et al.*, 2010]. All statistical analyses were conducted using Minitab 15 software and Matlab 2013a (MathWorks) for data processing and the tree regression analysis.

2.4. Identifying Upwelling Conditions for Case Studies

[20] Lower SST data ($\leq 14°$C) in combination with positive ΔpCO$_2$ (i.e., outgassing) was used to identify

upwelling events at the specific sites used in this study over the course of the year. A temperature of 14°C is the lower limit for the 95% confidence interval of the mean of SST for the year. Using physical variables (i.e., SST and wind speed), we selected three representative case studies in which all measured variables were available (SST, wind speed, $\Delta p CO_2$, and FCO_2 in both regions), but with distinct physical conditions in order to determine the dynamics and relationships between SST, wind speed, $\Delta p CO_2$, and FCO_2 during: (1) an upwelling event (days 80 through 83; March) with high wind speeds ($\geq$10 m s^{-1} out of the northwest), low SST ($\leq$14°C) and high positive $\Delta p CO_2$; (2) a relaxed upwelling period (days 257 through 260; August) with lower wind speed (<10 m s^{-1} out of the west), higher SST (>14°C) with low positive $\Delta p CO_2$; and (3) a mixed, upwelling/nonupwelling scenario (days 300 through 302; October) with higher wind speeds ($\geq$10 m s^{-1} out of the northwest), decreasing SST (approximately 18°C at the beginning of the case study going down to ~15°C by the end of the case study), and low positive $\Delta p CO_2$.

3. Results

3.1. Net FCO_2

[21] Data collected in the near-shore region was obtained for the entire calendar year of 2009 and was used to calculate an annual CO$_2$ budget. The net FCO_2 was calculated from the highest frequency data obtained from the mooring buoy and has as a unit of magnitude of mol m^{-2} y^{-1}. This region was an overall weak net source of CO$_2$ to the atmosphere with a FCO_2 of 0.043 mol m^{-2} y^{-1}; where 91% of the positive FCO_2 (outgassed from the ocean) was contributed during the upwelling season (days 106 through 222; Figure 3). The upwelling season may be seen in the tendency of the direction of the wind from March through September during this particular year (Figure 3c). Furthermore, the SST and $\Delta p CO_2$ indicate that the upwelling events were sporadic (Figure 3a) during the season. The spring bloom occurred from the middle of February through March (Figure 4d), during which there were relatively strong winds out of the northwest (Figures 3b and 4a) and low SSTs (Figure 3a) accompanied by low positive and negative FCO_2 (Figure 3e).

[22] Due to instrument failure, we are unable to report an annual net flux for the intertidal site. In situations where there is a lack of data, terrestrial studies using EC typically apply a gap-filling technique to determine the missing FCO_2 [*Moffat et al.*, 2007]. In this case, a gap-filling approach (e.g., artificial neural networks, MLR, lookup tables) is not possible because the missing data gaps are large (>4 months) and the environmental conditions for the missing data for the entire upwelling season were likely different from the data we were able to capture (i.e., shorter upwelling events as opposed to longer, sustained events). For shorter data gaps (no more than 1 day for low frequency data or two half-hour periods for high frequency data), we used linear interpolation to determine the missing FCO_2, otherwise the missing data is represented as a data gap (i.e., missing values). Our instrument failure happened to occur during the season where the most intense upwelling occurred (Figure 4).

3.2. Results of Regression Tree Analysis

[23] The regression tree for the intertidal zone (Figure 5a) shows that wind speed was the most import factor for predicting the FCO_2 (top node) and was able to predict 85% of the overall variability of FCO_2 (predicted-$R^2 = 0.85$; $p < 0.001$; $n = 86$; data includes the 3 case studies). Regardless of the $\Delta p CO_2$ value, the highest predicted FCO_2 (>25.77 μmol CO$_2$ m^{-2} s^{-1}) was influenced by wind speeds $\geq$9.75 m s^{-1}. Only at wind speeds of >5.51 m s^{-1} but <9.75 m s^{-1} was the $\Delta p CO_2$ an important factor for predicting the FCO_2. In this region, the SST (proxy for upwelling or gas solubility) was not a predictive factor for overall FCO_2.

[24] In the near-shore, the $\Delta p CO_2$ value (top node) was the most important factor for predicting the FCO_2 (Figure 5b). This regression tree predicted 86% of the overall variability of FCO_2 (predicted-$R^2 = 0.86$; $p < 0.001$; $n = 86$; data includes the 3 case studies). The highest predicted FCO_2 (mean of 8.68 μmol CO$_2$ m^{-2} s^{-1}) were due to a combination of high $\Delta p CO_2$ values (>29.28 ppm) and higher wind speeds ($\geq$5.49 m s^{-1}). In this region, the SST was important for predicting the FCO_2 when $\Delta p CO_2$ was <29.28 ppm, although at higher SST ($\geq$13.45°C) we found the lowest FCO_2 rates (mean of 0.010 μmol CO$_2$ m^{-2} s^{-1}).

3.3. Case Study 1 With Upwelling: High Winds, Low SST, and High Positive $\Delta p CO_2$

[25] For case study 1, the winds prevailed from the northwest (approximately 315°; Figure 4), there was no substantial stratification in the water column (Figure 2), and the SST was $\leq$14°C (Figure 6a); indicating upwelling conditions based on our criteria as well as those of previous studies [i.e., *Palacios et al.*, 2004]. The average $p CO_2$ during this case study was 426.3 ± 47.5 ppm ($n = 32$); $p CO_2$ was most variable (i.e., 11% change during this case study) during this period compared with the other two of the three cases. The FCO_2 in the intertidal zone was up to 4 orders of magnitude greater than that of the near-shore (Figure 6a). The MLR shows that in the intertidal zone, wind was more significant ($p < 0.001$) than either SST or $\Delta p CO_2$, whereas in the near-shore, $\Delta p CO_2$ was the most significant ($p < 0.001$) factor contributing to the variability of FCO_2 (Table 1). MLR analysis also shows that SST, wind speed, and $\Delta p CO_2$ explained 51% and 67% of the variability of FCO_2 in the intertidal zone and near-shore regions, respectively (Table 1). Cross correlation analysis in the intertidal zone shows that FCO_2 was in phase with wind speed (no lags; $r = 0.74$), while SST and $\Delta p CO_2$ showed negative correlations with longer lags (Table 2). For the near-shore, however, the FCO_2 was in phase with the SST and $\Delta p CO_2$ ($r = -0.68$ and 0.82, respectively), while there was a lag in relation to the wind (Table 2). The Chla was 9.23 mg m^{-3} during this case on the 81st day of the year (Figure 4d), and was 990% higher in comparison to values during non-upwelling conditions.

3.4. Case Study 2 Nonupwelling: Low Winds, High SST, and Low Positive $\Delta p CO_2$

[26] During case study 2 (Figure 6b), the SST was higher by approximately 3°C than during case study 1 and the winds were weaker by about 2 m s^{-1} and out of the west and east (wind from the east is not graphically represented
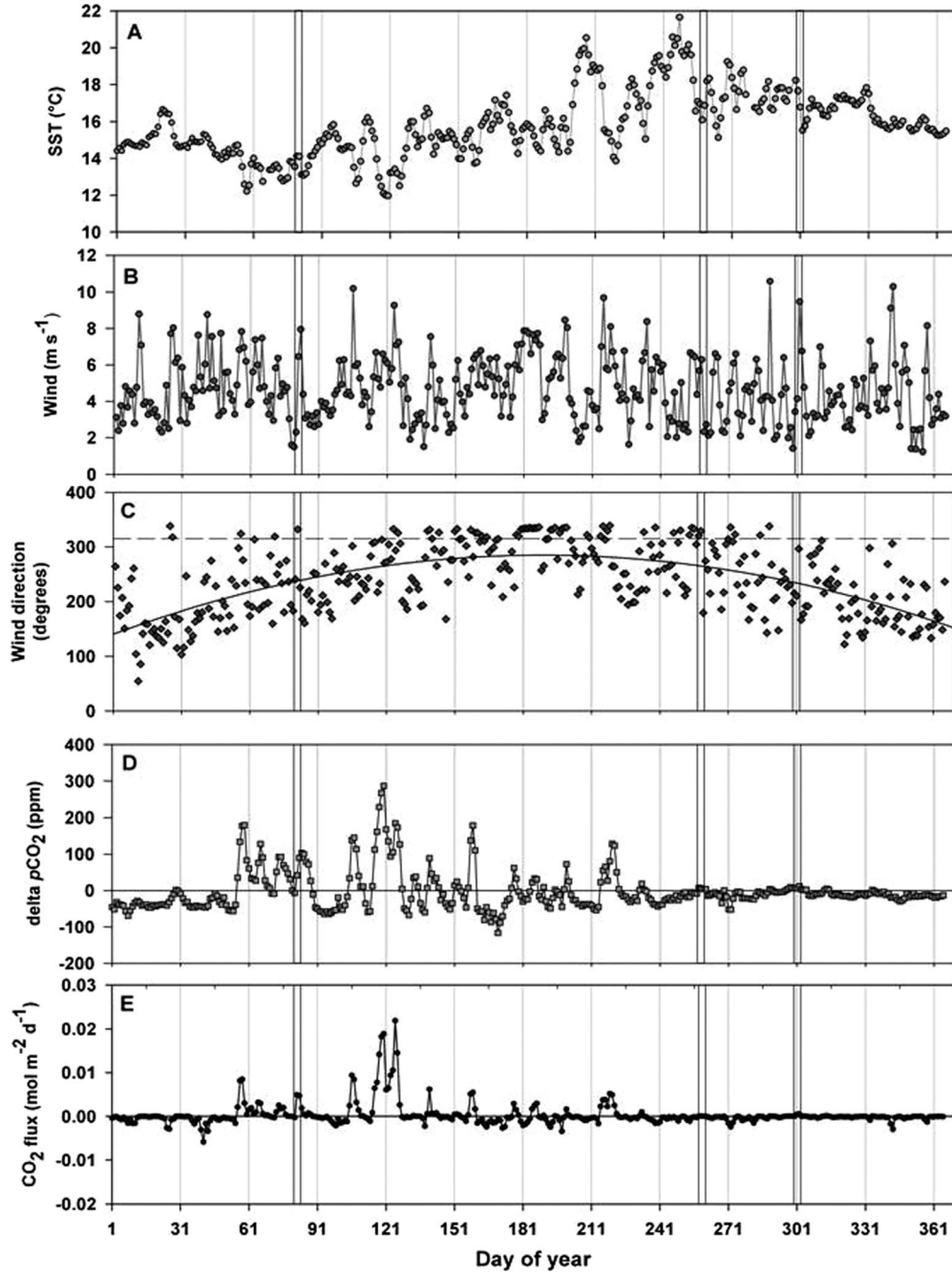
Figure 3. Daily averages for (a) sea surface temperature (SST); (b) wind speed; (c) wind direction; (s) ΔpCO$_2$; and (e) FCO$_2$ at the near-shore site for 2009. The solid black line in (c) shows general tendency of the wind direction, which originates from directions out of the northwest during the middle of the year (i.e., the "upwelling season"); the dashed horizontal black line represents 315°, or northwest, the wind direction which induces upwelling. Vertical dark grey lines at days 80 to 83, 257 to 260, and 300 to 302 represent the case studies, which are discussed in detail later on in the text.

as these data were filtered out as non-marine origin; Figure 4b). The higher SST values and temperature at depth indicate that the water column was stratified for this period (Figure S1, online only). During this case, the FCO$_2$ in both the near-shore and intertidal regions were lower by approximately 99% and 31%, respectively, than during case 1 (i.e., upwelling). The average pCO$_2$ during this case was the lowest of the 3 case studies (385.1 ± 12.4 ppm; $n = 32$) and var-

ied by 3.2% over the course of the case study. The Chla concentrations were lower than they were during the upwelling season (including case study 1) with a value of 1.03 mg m^{-3} on the 257th day of the year (Figure 4d).

[27] According to the MLR analysis, there were no significant relationships ($p > 0.05$) between SST, wind, or ΔpCO$_2$, and FCO$_2$ in the intertidal zone (Table 1). In the near-shore, the ΔpCO$_2$ was the most significant factor
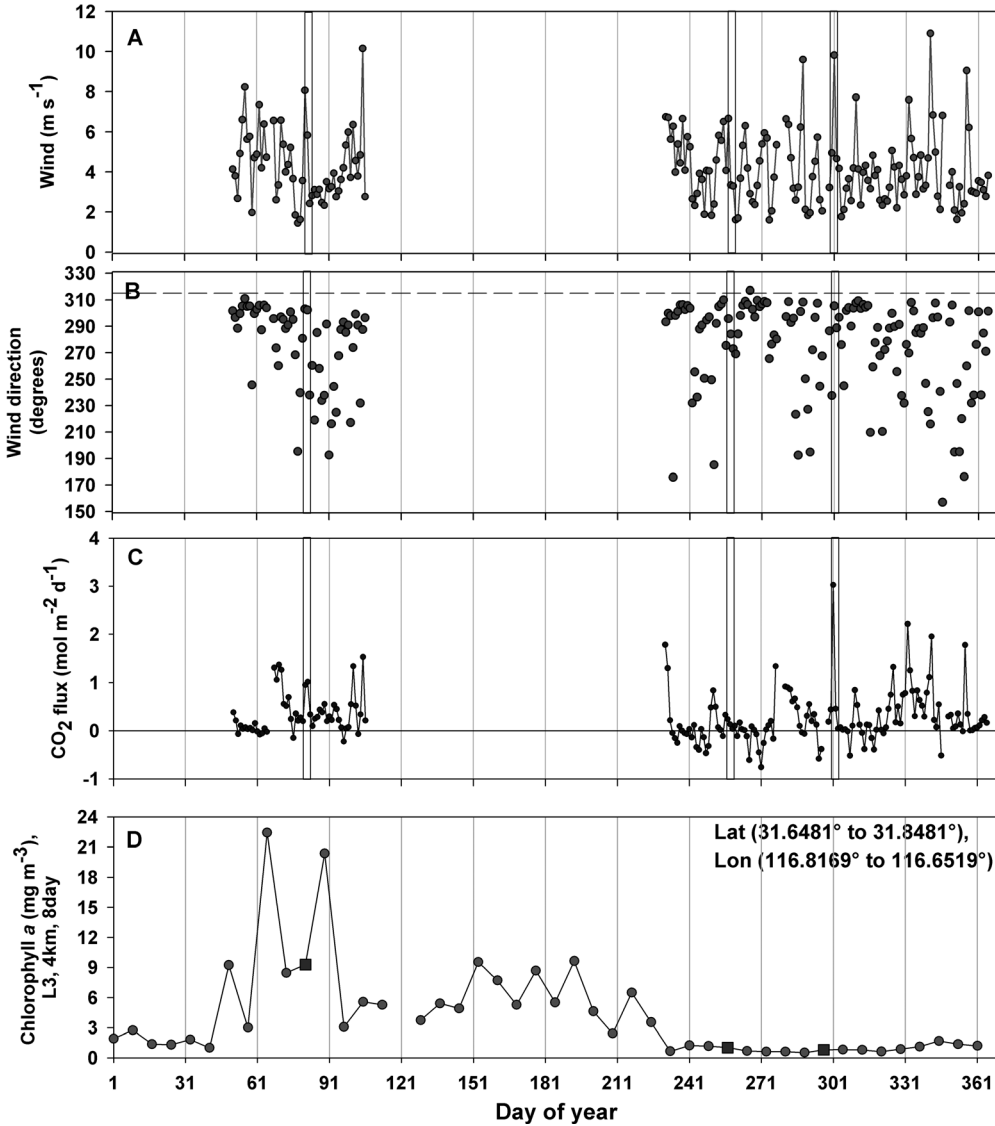
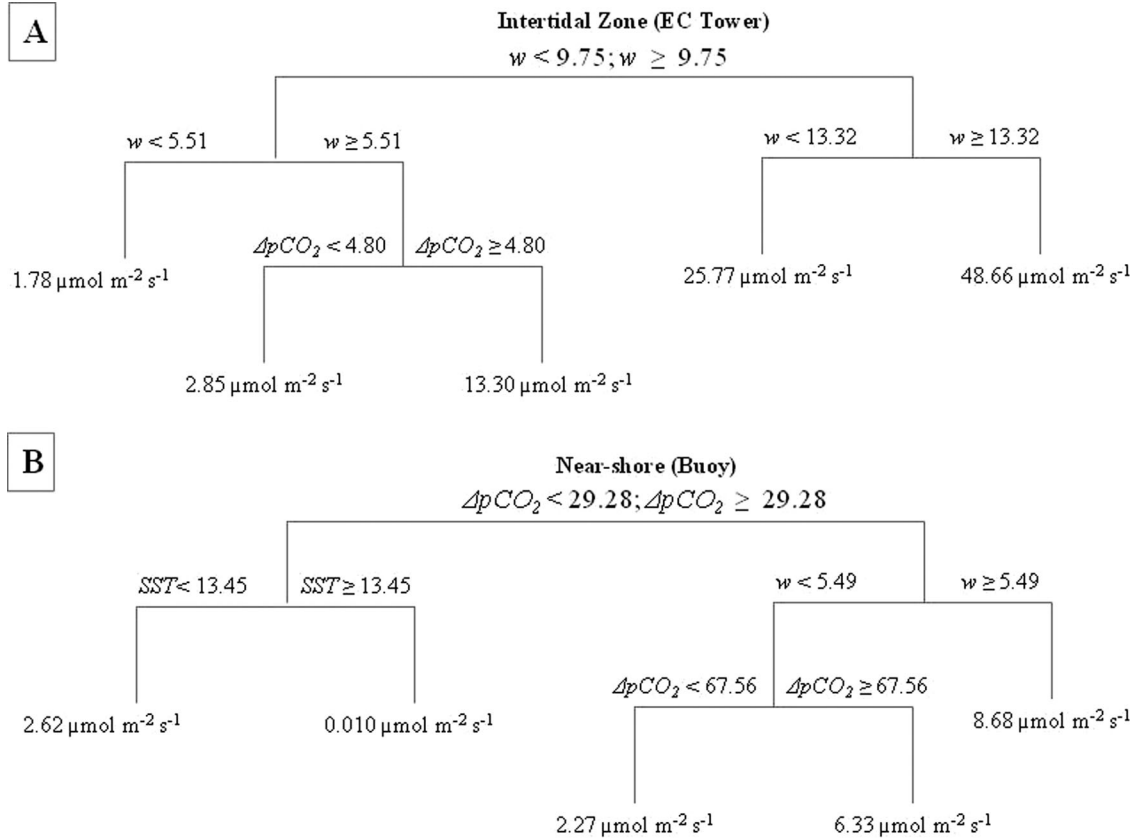**Figure 4.** Daily averages for (a) wind speed; (b) wind direction; (c) FCO$_2$ at the intertidal site; and (d) chlorophyll a (Chla) for 2009. The horizontal dashed black line in (c) represents 315°, or northwest, the wind direction that induces upwelling. Vertical dark grey lines at days 80 to 83, 257 to 260, and 300 to 302 represent the case studies, which are discussed in detail later on in the text. Grey boxes in (d) represent the dates closest to the case studies. The Chla data from SeaWiFS sensors was obtained for the study period from the NASA Giovanni server: http://disc.sci.gsfc.nasa.gov/giovanni/overview/index.html.

explaining the variability of FCO$_2$ ($p < 0.001$) while neither SST nor wind speed showed a significant relationship to FCO$_2$ ($p > 0.05$; Table 1).

[28] Cross correlation analysis shows that the lag between the wind and FCO$_2$ in the intertidal zone increased to 6 hours ($r = 0.32$), whereas this lag decreased in the near-shore to 3 hours ($r = 0.49$) from case study 1 (Table 2). The lag between SST and FCO$_2$ ($r = -0.65$) in the intertidal zone increased by 3 hours in comparison to case study 1. The r values all decreased (weaker relationship) except for SST versus FCO$_2$ in the near-shore ($r = 0.46$). In the intertidal zone, the ΔpCO$_2$ was negatively correlated to FCO$_2$ ($r = -0.31$) as in case study 1, but with a shorter lag of only 12 hours. In the near-shore, again the ΔpCO$_2$ was in phase with FCO$_2$ ($r = 0.74$).

3.5. Case Study 3 Mixed Scenario: High Winds, High SST, Low Positive ΔpCO$_2$

[29] In case study 3, the SST was 18°C but then decreased by 3°C by the end of the 3 days; the winds out of the northwest were between approximately 10 and 16 m s^{-1} (Figure 6c). The water column was stratified to approximately 30 m at IMECOCAL station 100.30 according to the temperature profile (Figure 2). The deep CO$_2$ rich waters, which were brought to the surface due to upwelling during case study 1 (when wind speeds were lower than the present case), were not present during case study 3. Furthermore, there were no large positive ΔpCO$_2$ values (Figure 6c) as there were in case study 1 but high positive FCO$_2$ in the intertidal zone. During this particular case, we observed the highest measured FCO$_2$ (up to almost 60

8

A Intertidal Zone (EC Tower)
$w < 9.75; w \geq 9.75$

$w < 5.51$ $\quad$ $w \geq 5.51$

$\Delta pCO_2 < 4.80$ $\quad$ $\Delta pCO_2 \geq 4.80$

1.78 µmol m^{-2} s^{-1}

2.85 µmol m^{-2} s^{-1} $\qquad$ 13.30 µmol m^{-2} s^{-1}

$w < 13.32$ $\quad$ $w \geq 13.32$

25.77 µmol m^{-2} s^{-1} $\qquad$ 48.66 µmol m^{-2} s^{-1}

B Near-shore (Buoy)
$\Delta pCO_2 < 29.28; \Delta pCO_2 \geq 29.28$

$SST < 13.45$ $\quad$ $SST \geq 13.45$

$w < 5.49$ $\quad$ $w \geq 5.49$

$\Delta pCO_2 < 67.56$ $\quad$ $\Delta pCO_2 \geq 67.56$

2.62 µmol m^{-2} s^{-1} $\qquad$ 0.010 µmol m^{-2} s^{-1}

8.68 µmol m^{-2} s^{-1}

2.27 µmol m^{-2} s^{-1} $\qquad$ 6.33 µmol m^{-2} s^{-1}

Figure 5. Results of the regression tree analysis for the intertidal (a) and near-shore (b) regions using the combined data of the three case studies when eddy covariance and buoy measurements were available. Where w is the wind speed (m s^{-1}), SST is the sea surface temperature (°C), and ΔpCO_2 is the air-sea CO$_2$ differential (ppm). Terminal nodes represent the mean predicted air-sea FCO_2.

µmol m^{-2} s^{-1}) in the intertidal zone, yet near neutral conditions in the near-shore (Figure 6c). The average pCO_2 for this case was 394.3 ± 6.19 ppm ($n = 24$) and only varied by 1.57% during this case study. The Chla, approximately 0.80 mg m^{-3} on the 297th day of the year (Figure 4d), is similar to case study 2.

[30] Results from the MLR analysis show that the wind and ΔpCO_2 were highly significant for both the intertidal zone and near-shore ($p = 0.001$ and $p < 0.001$, respectively) for explaining the variability in FCO_2 (74% and 80%, respectively; Table 1). During case study 3, the cross correlation shows that wind speed and FCO_2 were in phase ($r = 0.85$; Table 2) in the intertidal zone. In the near-shore, we still observe a relatively strong negative correlation between SST and FCO_2 with a 6 h lag ($r = -0.67$), even though the FCO_2 is weak. The ΔpCO_2 in the intertidal zone lagged 9 h behind the FCO_2 with a negative correlation ($r = -0.48$), while in the near-shore it was positively in phase with FCO_2 ($r = 0.79$).

4. Discussion

4.1. Net FCO_2

[31] The annual net FCO_2 for the near-shore in the Ensenada region for 2009 was close to neutral, suggesting that on this time scale in-water processes were the dominate control on the FCO_2 as well as advective and biological flow of carbon [*Pennington et al.*, 2009]. The weak net source of FCO_2 (0.043 mol m^{-2} y^{-1}) was likely due to the fact that the region along northern Baja California is characterized by CO$_2$ rich waters brought to the surface via Ekman driven upwelling with a strong meso-scale seasonal variation caused by the wind-induced upwelling (Figure 3b and 3c) [*Palacios et al.*, 2004]. The results of the net annual FCO_2 from buoy data in the present study are in general agreement with the results of the *Takahashi et al.* [2009] estimates for the closest point where the data was available: the given data indicates the region is close to neutral. The highest Chla values occurred during the early part of the upwelling season, but coincided with positive FCO_2 for the area that incorporates both the intertidal zone and near-shore; suggesting that the pCO_2 from upwelling was so high that biological uptake was insufficient to prevent outgassing of FCO_2 [*Smith and Hollibaugh*, 1993]. We are cautious to make any firm conclusions of the biological component of FCO_2 variability based on Chla from satellite data due to the low (8 days) temporal resolution of the data set [*Lueger et al.*, 2008].

4.2. Case Study 1 With Upwelling: High Winds, Low SST, and High Positive ΔpCO_2

[32] During case study 1 the wind speed was more important in the intertidal zone than in the near-shore for the
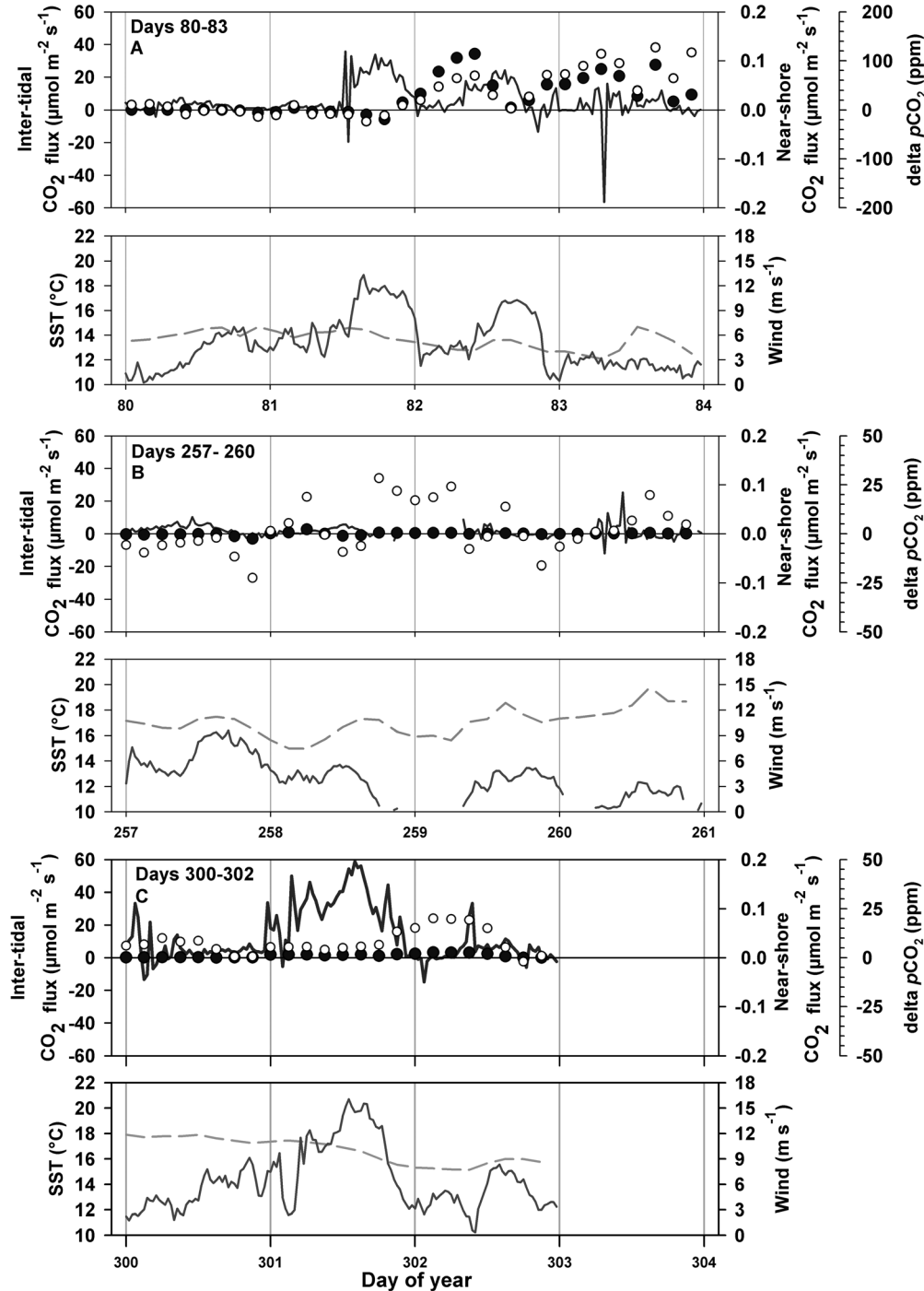
Figure 6. High temporal resolution time series for 3 distinct cases during 2009 from the intertidal (1 hour averages) and near-shore sites (3 hour intervals) for (a) days 80 through 83 (case study 1), (b) 257 through 260 (case study 2), and (c) 300 through 302 (case study 3). In the top panel for each case study, the solid line is the intertidal zone and the dots are the near-shore data: black dots are the FCO$_2$ and the white dots are the ΔpCO$_2$. In the bottom panel of each case study, the solid line is the wind speed (1 hour averages) and the dashed line is the SST (3 hour intervals). It should be noted that the scale for the near-shore FCO$_2$ and ΔpCO$_2$ in case study 1 is different than case studies 2 and 3. This was done in order to be able to see the behavior of FCO$_2$, as the magnitude of the values is smaller in case studies 2 and 3 than they are in case study 1.

explanation of the variability of FCO$_2$. Our results from MLR analysis suggest that the FCO$_2$ in the intertidal zone in the present study was more sensitive to physical

turbulence (wind speed) than the near-shore (Table 1). Physical mechanisms could involve the transfer velocity of CO$_2$ that is related to breaking waves, white capping [*Yelland et al.,*

Table 1. Results for Multiple Linear Regression Analysis for Both the Intertidal Zone and Near-Shore for the Three Explanatory Variables (ΔpCO_2, SST, and Wind) for the Control of FCO_2 Variability[a]

	p value	Adjusted R^2	Predicted R^2
Case 1			
Intertidal zone		0.51	0.41
SST	0.45		
Wind	**<0.001**		
ΔpCO_2	0.79		
Near-shore		0.67	0.62
SST	0.51		
Wind	0.31		
ΔpCO_2	**<0.001**		
Case 2			
Intertidal zone		0.05	0
SST	0.20		
Wind	0.42		
ΔpCO_2	0.57		
Near-shore		0.53	0.36
SST	0.16		
Wind	0.83		
ΔpCO_2	**<0.001**		
Case 3			
Intertidal zone		0.74	0.69
SST	0.12		
Wind	**<0.001**		
ΔpCO_2	0.05		
Near-shore		0.80	0.78
SST	0.14		
Wind	**0.001**		
ΔpCO_2	**<0.001**		

[a]Results in bold are statistically significant.

2009], the spray liberated from breaking waves [*de Leeuw et al.*, 2000], and finally bubble formation and dispersion [*Zhang*, 2012]. In the intertidal zone, the combination of waves (driven by the wind) and bathymetry may cause turbulence in the water column that is not present in the near-shore. The waves off Todos Santos Island are known for attracting surfers from all over the world; although there are presently no specific studies on the wave height on the windward side, it has been determined that the wave height within Todos Santos Bay (to the leeward side) is up to 2.5 times higher than at any other point along the Baja California Peninsula [*Martinez-Diaz-De-Leon*, 2004]. We therefore infer that the wave height on the windward side of the island is larger than the leeward side. Higher wind speeds, which cause white capping [*Yelland et al.*, 2009], are also important for the formation and dispersion of bubbles [*Norris et al.*, 2008]. As the bubbles disperse, they release sea spray (also created/enhanced by breaking waves), which is an important factor in the release of CO_2 from the ocean [*Zhang*, 2012]. Furthermore, *Norris et al.* [2008] showed a positive linear relationship between wind speed and particle flux (0.15 to 1.25 micron radius), thus suggesting the importance of sea spray on CO_2 release specifically in regions with high air turbulence. Inherently, there is more turbulence in an intertidal zone where waves are breaking than in a near-shore region. The regression tree analysis shows the importance of moderate wind speeds ($5.51 \leq w$ 13.32 m s^{-1}) even in the absence of higher ΔpCO_2 values (≥ 4.80 ppm; Figure 5a) when using the combined information of FCO_2 for all case studies.

Clearly, more studies on the influence of wind speed in relation to breaking waves in regulating FCO_2 are needed in intertidal regions around the world.

[33] Our results suggest that the FCO_2 in the near-shore, measured with the bulk gradient method, were less sensitive to the fast temporal dynamics and finer spatial scale processes influenced by changes in wind speed over the surface of the ocean as it is to meso-scale processes, such as upwelling (SST and ΔpCO_2; Table 2). In contrast, FCO_2 in the intertidal zone, measured by the EC method, were more sensitive to the influence of wind speed on the fast temporal dynamics and fine spatial scale processes (such as wind; Table 2). It should be pointed out that the wind speed data used to calculate the FCO_2 is the 30 minute average for the intertidal zone and the 3 h average for the near-shore. This averaging inherently will influence the near-shore results to appear less sensitive to micro-scale processes; therefore, high temporal resolution measurements are needed to accurately calculate the nonstationary influence of physical forcing [*Katul et al.*, 1994].

[34] Upon further investigation into the reason for the several magnitude difference in FCO_2 between the sites, we used the salinity data from the April 2009 IMECOCAL cruise (Figure S2, online only) and found that the windward side of Todos los Santos Island was located in the California Current (characterized by low salinity and pCO_2 in comparison to surrounding surface water and other water masses present throughout the region [i.e., *Takesue and van Geen*, 2002]); whereas, the near-shore was located within an upwelling zone confined close to the coastline. The regression tree shows that the overall lower ΔpCO_2 values that are associated with waters of the California Current in the near-shore are not the most important driver for overall larger FCO_2 in the intertidal zone (Figure 5a). Even though lower pCO_2 values are occurring in the intertidal zone in

Table 2. Results of Cross Correlation Analysis for Both the Near-Shore and Intertidal Zone[a]

	Correlation (r)	Time Lag (Hours)
Case 1		
Wind vs intertidal	0.74	0
Wind vs near-shore	0.64	15
SST vs intertidal	−0.58	15
SST vs near-shore	−0.68	0
ΔpCO_2 vs intertidal	−0.39	21
ΔpCO_2 vs near-shore	0.82	0
Case 2		
Wind vs intertidal	0.32	6
Wind vs near-shore	0.49	3
SST vs intertidal	−0.65	18
SST vs near-shore	0.46	3
ΔpCO_2 vs intertidal	−0.31	12
ΔpCO_2 vs near-shore	0.74	0
Case 3		
Wind vs intertidal	0.85	0
Wind vs near-shore	0.67	15
SST vs intertidal	0.69	18
SST vs near-shore	0.67	6
ΔpCO_2 vs intertidal	−0.48	9
ΔpCO_2 vs near-shore	0.79	0

[a]All cross correlations were significant at $p < 0.05$.

the California Current, the FCO$_2$ is higher than the near-shore. This phenomenon may be explained by the fact that wind (which explains the majority of variance in the intertidal zone) enhanced turbulence and caused the release of more CO$_2$ than the air-sea differential (ΔpCO$_2$) alone as in the near-shore; further highlighting the importance of future research to determine the transfer function for wave turbulence in the intertidal zone and how it likely differs from the near-shore and open ocean. We are presently unaware of studies that have determined a transfer function specifically for high energy intertidal waters.

[35] The distinct water masses at the two sites may also explain why we only found a positive correlation between ΔpCO$_2$ and FCO$_2$ in the near-shore and not in the intertidal zone (Table 2). Because the upwelling core was isolated in the region where the buoy is located, the effect of the ΔpCO$_2$ due to upwelling (seen as a positive correlation) was not necessarily detectable in the intertidal zone. This result suggests that horizontal advective processes may be important for the transport of high concentrations of CO$_2$ [*Pennington et al*., 2009] into the intertidal zone from the near-shore where the turbulent energy was the principle factor for its liberation into the atmosphere. According to IMECOCAL salinity data, we did not see evidence of high pCO$_2$ waters in this region. It is not possible to have in situ pCO$_2$ data in the intertidal zone, at this time, due to the presence of large waves and rocky shores, which will destroy the equipment and threaten the lives of the researchers.

4.3. Case Study 2 Nonupwelling: Low Winds, High SST, and Low Positive ΔpCO$_2$

[36] During this case study, we did not see evidence of upwelling at either site. This is demonstrated by the higher SST values during this case study, in comparison to case study 1, implying that the cold CO$_2$ rich deep waters from upwelling were not reaching the surface. Therefore, the FCO$_2$ representing outgassing from the ocean was not as high as during periods with weaker water column stratification (upwelling). Even though there was no evidence of upwelling reaching the surface ocean during this period, there were no substantial negative FCO$_2$ values that would indicate uptake; this may have been due to the decreased solubility of CO$_2$ at higher SSTs [*Sarmiento and Gruber*, 2006]. Another possible reason for near neutral FCO$_2$ may have been due to sufficient uptake by biological processes of the low pCO$_2$ associated with nonupwelling conditions at this time of the year. Even though the Chla was low in comparison to the rest of the year (Figure 6b), the ΔpCO$_2$ was also relatively low, indicating that biologically mediated processes (i.e., bacterial remineralization and photosynthesis) may have been responsible for controlling the variability of FCO$_2$ [*Bianchi et al*., 2009]. This hypothesis, however, would require further investigation as we did not measure the variables necessary to determine the direct biological uptake and release of CO$_2$.

[37] In case study 1, the majority of FCO$_2$ variability could be explained by wind in the intertidal zone (Table 1), however, in case study 2, the wind was not a significant factor in explaining the variability of FCO$_2$ at either site. Moreover, the MLR results are not significant for explaining any of the variability in the intertidal zone (Table 1). In

contrast, for the near-shore the MLR was significant for case study 2 where ΔpCO$_2$ was the most important factor explaining over 50% of the variability of FCO$_2$ (Table 1). It is likely that the physical differences in the two regions are responsible for the fact that MLR may only explain variability in one region (see discussion below). These results suggest that the parsimony principle for using a linear model is useful to represent a large proportion of the variability of FCO$_2$, but during some specific conditions other unmeasured variables or an unrepresented nonlinear process controls FCO$_2$ in the intertidal zone.

[38] Cross correlation analysis suggests that during this nonupwelling scenario the relationships between physical forcing variables and FCO$_2$ were not as pronounced as during upwelling (case study 1; Table 2). The longer lags suggest that in the absence of upwelling the FCO$_2$ did not respond as rapidly to physical forcing variables. During this case, even though FCO$_2$ is close to neutral, the majority of the data points were slightly positive and indicated outgassing (Figure 5b). The increased SST during this case study may have promoted the outgassing of FCO$_2$ due to the decreased solubility of CO$_2$ in warmer waters [*Sarmiento and Gruber*, 2006]. In the near-shore, similar to the results of SST, the correlation is positive for ΔpCO$_2$, although the lag is longer, suggesting that in the absence of upwelling the FCO$_2$ in this region did not respond as quickly to the ΔpCO$_2$ as it did when upwelling was occurring.

4.4. Case Study 3 Mixed Scenario: High Winds, High SST, Low Positive ΔpCO$_2$

[39] The almost neutral values of ΔpCO$_2$ during case study 3 suggest that the presence of upwelled deep CO$_2$ rich waters may not always be a requisite for larger outgassing of FCO$_2$ in the intertidal zone. In fact, during October 2009, waters with characteristics of the California Current (which inherently have lower pCO$_2$ than upwelled waters [*Feely et al*., 2008]) were found at the near-shore site (Figure S2, online only), while Todos Santos Island was characterized by waters with a higher salinity (likely due to evaporation in the surface layer), which, in combination with the water column temperature (Figure 2), suggests that intertidal zone was stratified, at least at the beginning of the case study. *Linacre et al*. [2010] also described this occurrence of the California Current close to the coast during periods of relaxed upwelling. In this case, the outgassing FCO$_2$ in the intertidal zone was higher than any other case study at either site, even during the upwelling season (Figure 3). Furthermore, based on the salinity data from the IMECOCAL cruise, it is not likely that CO$_2$ rich waters were being advected from surrounding water masses, as the given salinity data are indicative of the California Current and its counter flows [*Linacre et al*., 2010]. Because we use SST in combination with high ΔpCO$_2$ as an indicator of upwelling, we see that these criteria were not met during this case study and that in the absence of upwelling the SST and wind (which was higher during this case study than the other two) became even more important for regulating the variability of FCO$_2$ (Table 1). According to the results for the MLR in the intertidal zone, wind (and associated turbulence) explained the majority of the variation of FCO$_2$ (between 74% and 80%), followed by ΔpCO$_2$ (Table

1). The aforementioned relationship between particle size (sea spray) and wind friction [*Norris et al.*, 2008] were likely the controls for FCO$_2$, even though upwelling is not occurring.

[40] The weaker FCO$_2$ observed during this case study in the near-shore in comparison to case study 1 were due to the absence of CO$_2$ rich waters; and in comparison to the intertidal zone during the same time of year were likely due to weaker influence from turbulent processes (waves) driven by wind. Based on these results, we hypothesize that spray will be more important where waves break and crash on rocks, and therefore drive the higher FCO$_2$ values that we found in the intertidal zone. We encourage further studies on this potential effect across upwelling zones and rocky shores to test this hypothesis.

[41] Satellite Chla was relatively low and constant before, during, and after this case study, suggesting that for both sites there is little evidence to assume that the positive FCO$_2$ was principally due to high rates of biological activity [*Smith*, 1981]. As in case study 2, because Chla and ΔpCO$_2$ were lower than during other times of the year, it is likely that the high positive FCO$_2$ values (outgassing) were primarily influenced by wind forced turbulence. Because the p value for SST in both regions is not significant, then we assume that neither upwelling nor the effect of SST on solubility was contributing to the variability of FCO$_2$. Even in the absence of high positive ΔpCO$_2$ values, which are associated with outgassing during upwelling, we found high positive FCO$_2$, thus highlighting the important role of the wind (and wind-driven turbulence) in the liberation of CO$_2$ from intertidal zone waters. In the near-shore, we find that again there is a positive cross correlation between SST and FCO$_2$ indicating that the relationship between FCO$_2$ was not driven by upwelling (Table 2) or gas solubility into lower SST in this case. Furthermore, the lag for FCO$_2$ versus SST was longer in this case than the other two suggesting weaker coupling, while the results for the wind are similar to those during upwelling (case study 1; Table 2).

4.5. Spatial Variation Across Continental Margins

[42] We find that the FCO$_2$ was always higher in the intertidal zone than in the near-shore. The MLR and regression tree approaches agree that the most important forcing variables for influencing FCO$_2$ rates are different at the two sites. Even if we assume a homogeneous distribution of pCO$_2$ between the two sites, we postulate that breaking waves and wind would be the most likely factors contributing to this spatial difference. Wave heights during the study period were between 1.5 and 4.5 m and it is assumed that in the break zone the wave height (enhanced by steep sloping bathymetry) was higher than the reported wave height by the model output as well as in the near-shore site. Because the wave height is actually greater in the intertidal zone than the near-shore, it was likely amplifying the FCO$_2$ due to increased turbulence [*Zhao et al.*, 2003]. Specifically for case study 3, the wave turbulence was important because the California Current was found close to the coast and is inherently lower in pCO$_2$ than upwelled waters. Bathymetry-enhanced wave height was not a factor in the near-shore, which is characterized by deep waters ($\geq$90 m) without breaking waves, only occasional white capping, and, most importantly, pCO$_2$ from upwelling

(during case study 1). In the intertidal zone, the wind (and related physical processes) played a clearer role in the variability of FCO$_2$ than in the near-shore. According to IME-COCAL water column data, it is not likely that the actual pCO$_2$ concentrations were homogeneous over the study region, but were lower in the intertidal zone where the greater fluxes were observed (Figure 6 and Supplementary Figure 2, online only). These results suggest the importance of the physical turbulence (and biological processes of intertidal regions; not measured in the present study) as primary biophysical drivers for liberating CO$_2$ from the surface ocean.

[43] Ocean processes controlling FCO$_2$ are complex but we were able to explain between 50% and 80% of the variability in FCO$_2$ using an MLR in most cases, and nearly 90% of the variability when we combined all case studies and used a tree regression approach. Only in the intertidal zone during case study 2 the MLR approach explained <50% of the variability (Table 1). Other studies have used this linear approach to determine the influence of different variables on the variability of FCO$_2$. For example, *Jiang et al.* [2008] using linear regression concluded that the SST explains most of the observed seasonal variation in FCO$_2$. *Boehme et al.* [1998] also reported a similar finding using a linear regression model as well as pointed out that nonlinear relationships are difficult to accurately discern, while other studies have highlighted the importance of quantifying nonlinear processes [*Bates and Merlivat*, 2001]. We use the MLR and regression tree approaches as methods to show that different biophysical processes influence the variability in FCO$_2$ as represented by the relevance of each measured variable for each case study and across the overall measurements. Our results show the need for the separation of regions to accurately and precisely determine the dynamics of CO$_2$ along continental margins as forcing variables exert differing influences over FCO$_2$ within this region.

[44] The variables measured in the present study alone cannot explain why higher FCO$_2$ is always seen in the intertidal zone. Typically, there is a steep gradient for ΔpCO$_2$ extending offshore, which has, in part, been attributed to biological controls [*Torres et al.*, 1999, 2003; *Friederich et al.*, 2008]. This would suggest that biological components exert varying degrees of the control of variability over FCO$_2$ both spatially and temporally. In the present study, due to the location of upwelling (Supplementary Figure 2, online only) in the near-shore, the ΔpCO$_2$ (which includes the biological component) is more statistically significant for the explanation of variability than in the intertidal zone. Therefore, specific site variability of unaccounted factors (biological and physical) may play an important role in the FCO$_2$ and nonlinear processes should be incorporated in further near-shore and intertidal zones studies.

[45] Our results indicate substantial spatial differences of FCO$_2$ across the continental margin influenced by the California Current and upwelling. These results are supported by previous studies not only for the regions affected by the California Current, but for various other regions; for example, *Boehme et al.* [1998], off the northeast coast of the United States, found that FCO$_2$ decreased offshore and that inner and outer shelf regions varied on different time scales. This was also the case for our near-shore and

intertidal regions based on the response to different physical and biological mechanisms (cross correlation analysis; Table 2). Another study conducted by *Jiang et al.* [2008] in the South Atlantic Bight, concluded that there were substantial spatial differences offshore in the FCO$_2$ due to SST and autotrophic respiration. The two previously mentioned studies indicate that SST and biological factors are the most important controlling mechanisms, while *Vandemark et al.* [2011] determined that FCO$_2$ on the inner shelf of the Gulf of Maine were greater than those farther from the coast (but still within the gulf) due to tidal mixing and wind stress. The different mechanisms documented as relevant controls of the FCO$_2$ show the importance of identifying the relevance of the various forcing mechanisms across temporal and spatial scales in the near-shore and intertidal regions. The present study shows that even when it appears that biological and chemical properties of the water column are similar across sties, it is the different physical processes that drive the direction and magnitude of FCO$_2$.

4.6. Limitations and Future Considerations

[46] Using an underway EC system in the open ocean *Kondo and Tsukamoto* [2007] showed that FCO$_2$ calculated using the bulk gradient method (with the formulation of *Liss and Merlivat* [1986] and the transfer velocity of *Wanninkhof* [1992] based on tracer experiments) was lower than the EC method by up to three orders of magnitude. Because the bulk formulation of *Wannikhof and McGillis* [1999] for the transfer velocity (k) used in this study was calibrated using EC measurements of FCO$_2$, we assume that our measurements of FCO$_2$ in the near-shore were also picking up all the features of the EC tower measurements in the intertidal zone. Therefore, the most likely reason for greater FCO$_2$ in the intertidal zone is not, in fact, due to the use of different measurement techniques, as was the conclusion of *Kondo and Tsukamoto* [2007], but due to actual greater FCO$_2$ (higher magnitude) in this region. We recognize that this interpretation must be validated at multiple sites around the world. The similar results (i.e., spatial differences) found in the present study as well as those by *Boehme et al.* [1998], *DeGrandpre et al.* [1998], *Jiang et al.* [2008], *Leinweber et al.* [2009], and *Vandemark et al.* [2011], may indicate the importance of the precise sampling location in terms of the physical turbulence generated in the water column by wind, waves, and tides and not necessarily the pertinence of the method used.

[47] Apart from the difference in magnitude of FCO$_2$ between the two regions, another important feature is the fact that the cross correlation results between ΔpCO$_2$ and FCO$_2$ in the intertidal zone were negative during the 3 case studies, while this relationship was positive in the near-shore (Table 2). This could be due to the fact that the ΔpCO$_2$ data in the present study are from the near-shore and the negative cross correlation result for the intertidal zone was because of the spatial difference (i.e., no actual relationship). Furthermore, the general behavior of these two variables in the intertidal zone is opposite (Figure 6) suggesting that the ΔpCO$_2$ in this study was not the same in the intertidal zone and near-shore. This could be a result of feedbacks and nonlinear processes not measured or explored in this study. We suggest that future studies include more continuous measurements of physical and biological variables that

could be used within a data-model-fusion approach to improve our understanding and predicting capability of FCO$_2$ across the continental margins.

[48] Another argument to warrant further study into the separation of intertidal and near-shore regions when determining an annual net FCO$_2$ is that the detail that is seen in the high frequency data measurements from the EC tower are not seen in the data from the buoy. The temporal resolution of the buoy in the present study is not as high as the EC tower and may lead to under or overestimations of the FCO$_2$ for the region because it is not well represented by the location of a single study site. It is also likely that a resolution of only 3 h in the near-shore is not fast enough to measure some of the larger fluctuations that are seen in the near-shore zone related to wind gusts or mid-day increases (Figure 6) and therefore underestimate the FCO$_2$. In light of the results in the present work, which shows that the FCO$_2$ in the near-shore region is not as sensitive to the wind as those in the intertidal zone, it is even more important to determine why two sites so close together present distinct FCO$_2$. It has been well established that the intertidal ocean presents typically greater FCO$_2$ (both for outgassing and uptake) than the open ocean (i.e., *Frankignoulle and Borges*, 2001; *Thomas et al.*, 2004; *Borges*, 2005; *Vandemark, et al.*, 2011), and it is therefore essential to clarify for scaling studies where the "intertidal zone" ends and "open ocean" like characteristics begin. Furthermore, reporting the annual net FCO$_2$ for different regions of the ocean will help to reduce the uncertainty in global FCO$_2$ estimates.

5. Conclusions

[49] The results presented here suggest that there are large differences in FCO$_2$ within the 3 km of ocean from the coast over the continental margin influenced by the California Current. Due to the dynamics in the region of the continental margin, it is likely that the annual budgets are different between the two sites observed in this study and that the annual FCO$_2$ presented here for the near-shore is not a good representation of the whole coastal region (near-shore and intertidal zones). The near-shore in this study is more heavily influenced by meso-scale processes (SST and ΔpCO$_2$ from upwelled waters) and likely reflects a larger spatial scale ocean CO$_2$ budget rather than is inclusive of our intertidal zone. In the intertidal zone, even in the absence of high ΔpCO$_2$ values driven by upwelling, wind (and wind-driven physical processes) created significantly larger and positive FCO$_2$ (outgassing). Differences in the FCO$_2$ are primarily due to the different physical processes at the two sites. MLR and regression tree analyses provide insight into the complexity of the processes driving FCO$_2$ over the continental margin. The MLR model does not account for the nonlinear processes, but the regression tree is an alternative approach to visualize the interaction among variables that influence FCO$_2$. Therefore nonlinear approaches are needed to study the details of interactions and feedbacks across this region. The distinct FCO$_2$ in the two regions studied is likely due to turbulent energy with a secondary affect due to the bathymetry. Separation of the intertidal zone into the breaker zone and non-breaker zone may also be necessary for regions with high surf to better

estimate FCO$_2$. Uncertainties of FCO$_2$ on the continental margins are likely due to spatial differences, which stem from different physical controls of variability over FCO$_2$ and are especially important in the absence of high ΔpCO$_2$ values due to upwelling. We encourage the scientific community to derive a parameterization for the transfer velocity of CO$_2$ over intertidal zones as it is likely different from that used in typical applications of the bulk method. Future research along continental margins should consider paired studies for determining FCO$_2$. We do not consider one method to be better than the other, but that each serves a different purpose. The EC tower may provide a greater range for a study area (i.e., larger footprint for measurements) and could be used to include the dynamic intertidal zone (due to the high sampling frequency), but will require more maintenance (cleaning and calibration) than a mooring buoy. Larger memory cards and a faster sampling protocol that includes multiple sensors will allow solving for fast ocean-atmosphere dynamics using both methods. Further analysis of the difference between mooring buoy and the EC methods are needed to reduce uncertainty between these two methods along continental margins across the world. Finally, this manuscript shares the vision of systematic carbon cycle observations across the continental margin of Mexico (as well as other global regions), and calls for the need of implementing a long term land-sea carbon cycle science program [*Vargas et al.*, 2012, 2013].

References

Alin, S., et al. (2012), Coastal carbon synthesis for the continental shelf of the North American Pacific Coast (NAPC): Preliminary results, *Ocean Carbon Biogeochem.*, *5*, 1–5.

Bakun, A. (1975), Daily and weekly upwelling indices, west coast of North America, 1967-73. U.S. Dep. Commer., NOAA Tech. Rep., NMFS SSRF-693, 114 pp.

Baldocchi, D., et al. (2001), FLUXNET: A new tool to study the temporal and spatial variability of ecosystem–scale carbon dioxide, water vapor, and energy flux densities, *Bull. Amer. Meteorol. Soc.*, *82*, 2415–2434.

Barton, A., B. Hales, G. G. Waldbusser, C. Langdon, and R. A. Feely (2012), The Pacific oyster, Crassostrea gigas, shows negative correlation to naturally elevated carbon dioxide levels: Implications for near-term ocean acidification effects, *Limnol. Oceanogr.*, *57*, 698–710.

Bates, N. R. (2006), Air-sea CO$_2$ fluxes and the continental shelf pump of carbon in the Chukchi Sea adjacent to the Arctic Ocean, *J. Geophys. Res.*, *111*, C10013, doi:10.1029/2005JC003083.

Bates, N. R., and L. Merlivat (2001), The influence of short-term wind variability on air-sea CO$_2$ exchange. *Geophys. Res. Lett.*, *28*, 3281–3284.

Bianchi, A. A., D. R. Pino, H. G. I. Perlender, A. P. Osiroff, V. Segura, V. Lutz, M. L. Clara, C. F. Balestrini, and A. R. Piola (2009), Annual balance and seasonal variability of air-sea CO$_2$ fluxes in the Patagonia Sea: Their relationship with fronts and chlorophyll distribution, *J. Geophys. Res.*, *114*, C03018, doi: 10.1029/2008JC004854.

Boehme, S. E., C. L. Sabine, and C. E. Reimers (1998), CO$_2$ fluxes from a coastal transect: A time-series approach. *Mar. Chem.*, *63*, 49–67.

Borges, A. V. (2005), Do we have enough pieces of the jigsaw to integrate CO$_2$ fluxes in the coastal ocean? *Estuaries*, *28*, 3–27.

Borges, A. V., B. Delille, and M. Frankignoulle (2005), Budgeting sinks and sources of CO$_2$ in the coastal ocean: Diversity of ecosystems counts, *Geophys. Res. Lett.*, *32*, L14601, doi:10.1029/2005GL023053.

Borges, A. V., et al. (2009), A global sea surface carbon observing system: inorganic and organic carbon dynamics in coastal oceans, in *Proceedings of OceanObs'09: Sustained Ocean Observations and Information for Society*, vol. *2*, edited by J. Hall, D. E. Harrison and D. Stammer, Venice, Italy, 21–25 September 2009, ESA Publication WPP-306, doi:10.5270/OceanObs09.cwp.07.

Breiman, L., J. H. Friedman, R. A. Olshen, and C. J. Stone (1984), *Classification and Regression Trees*, Wadsworth and Brooks/Cole, Monterey, California.

Cai, W.-J., M. Dai, and Y. Wang (2006), Air-sea exchange of carbon dioxide in ocean margins: A province-based synthesis, *Geophys. Res. Lett.*, *33*, L12603, doi:10.1029/2006GL026219.

Chavez, F. P., J. Ryan, S. E. Lluch-Cota, and C. Miguel Ñiquen (2003), From anchovies to sardines and back: Multidecadal change in the Pacific Ocean, *Science*, *299*, 217–221.

DeGrandpre, M. D., T. R. Hammar, and C. D. Wirick (1998), Short-term pCO$_2$ and O2 dynamics in California coastal waters, *Deep Sea Res., Part II*, *45*, 1557–1575.

De La Cruz-Orozco, M., J. Valdéz-Holguín, G. Gaxiola-Castro, M. Mariano-Matías, and T. Espinosa-Carreón (2010), Flujos de CO$_2$ océano-atmósfera, in *Dinámica del ecosistema pelágico frente a Baja California 1997–2007*, edited by G. Gaxiola-Castro, R. Durazo, 505 pp., Secretaría de Medio Ambiente y Recursos Naturales, México.

de Leeuw, G., F. P. Neele, M. Hill, M. H. Smith, and E. Vignati (2000), Production of sea spray aerosol in the surf zone, *J. Geophys. Res.*, *105*, 29,397–29,409, doi:10.1029/2000JD900549.

Edson, J. B., C. W. Fairall, L. Bariteau, C. J. Zappa, A. Cifuentes-Lorenzen, W. R. McGillis, S. Pezoa, J. E. Hare, and D. Helmig (2011), Direct covariance measurement of CO$_2$ gas transfer velocity during the 2008 Southern Ocean Gas Exchange Experiment: Wind speed dependency, *J. Geophys. Res.*, *116*, C00F10, doi:10.1029/2011JC007022.

Feely, R. A., C. L. Sabine, J. M. Hernandez-Ayon, D. Ianson, and B. Hales (2008), Evidence for upwelling of corrosive ''acidified'' water onto the continental shelf, *Science*, *320*, 1490–1492.

Frankignoulle, M., and A. V. Borges (2001), European continental shelf as a significant sink for atmospheric carbon dioxide. *Global Biogeochem. Cycles*, *15*, 569–576.

Frankignoulle, M., G. Abril, A. Borges, I. Bourge, C. Canon, B. Delille, E. Libert, and J.-M. Théate (1998), Carbon dioxide emissions from European estuaries, *Science*, *282*, 434–436.

Friederich, G. E., P. G. Brewer, R. Herlien, and F. P. Chavez (1995), Measurements of sea surface partial pressure of CO$_2$ from a moored buoy. *Deep-Sea Res., I 42*, 1175–1186.

Friederich, G. E., P. M. Walz, M. G. Burczynski, and F. P. Chavez (2002), Inorganic carbon in the central California upwelling system during the 1997–1999 El Niño-La Niña event, *Prog. Oceanogr.*, *54*, 185–203.

Friederich, G. E., J. Ledesma, O. Ulloa, and F. P. Chavez (2008), Air-sea carbon dioxide fluxes in the coastal southeastern tropical Pacific, *Prog. Oceanogr.*, *79*, 156–166.

Gattuso, J.-P., D. Allemand, and M. Frankignoulle (1999), Photosynthesis and calcification at cellular, organismal and community levels in coral reefs: A review on interactions and control by carbonate chemistry. *Am. Zool.*, *39*, 160–183.

Grachev, A. A., L. Bariteau, C. W. Fairall, J. E. Hare, D. Helmig, J. Hueber, and E. K. Lang (2011), Turbulent fluxes and transfer of gases from ship-based measurements during TexAQS 2006, *J. Geophys. Res.*, *116*, D13110, doi: 10.1029/2010JD015502.

Ho, D. T., C. S. Law, M. J. Smith, P. Schlosser, M. Harvey, and P. Hill (2006), Measurements of air-sea gas exchange at high wind speeds in the Southern Ocean: Implications for global parameterizations, *Geophys. Res. Lett.*, *33*, L16611, doi:10.1029/2006GL026817.

Jiang, L.-Q., W.-J. Cai, R. Wanninkhof, Y. Wang, and H. Lüger (2008), Air-sea CO$_2$ fluxes on the U.S. South Atlantic Bight: Spatial and seasonal variability, *J. Geophys. Res.*, *113*, doi: 10.1029/2007JC004366.

Katul, G. G., M. B. Parlange, and C. R. Chu (1994), Intermittency, local isotropy, and non-Gaussian statistics in atmospheric surface-layer turbulence, *Phys. Fluids*, *6*, 2480–2492.

Kondo, F., and O. Tsukamoto (2007), Air-sea CO$_2$ flux by eddy covariance technique in the equatorial Indian Ocean, *J. Oceanogr.*, *63*, 449–456.

Koné, Y. J. M., G. Abril, K. N. Kouadio, B. Delille, and A. V. Borges (2009), Seasonal variability of carbon dioxide in the rivers and lagoons of Ivory Coast (West Africa), *Estuaries Coasts*, *32*, 246–260.

Laruelle, G. G., H. H. Dürr, C. P. Slomp, and A. V. Borges (2010), Evaluation of sinks and sources of CO$_2$ in the global coastal ocean using a spatially-explicit typology of estuaries and continental shelves, *Geophys. Res. Lett.*, *37*, L15607, doi:10.1029/2010GL043961.

Leinweber, A., N. Gruber, H. Frenzel, G. E. Friederich, and F. P. Chavez (2009), Diurnal carbon cycling in the surface ocean and lower atmosphere of Santa Monica Bay, California, *Geophys. Res. Lett.*, *36*, L08601, doi:10.1029/2008GL037018.

Leuning, R. (2007), The correct form of the Webb, Pearman and Leuing equation for eddy fluxes of trace gases in steady and non-steady state, horizontally homogeneous flows, *Boundary Layer Meteorol.*, *123*, 263–267, doi:10.1007/s10546-006-9138-5.

Linacre, L., R. Durazo, J. M. Hernández-Ayón, F. Delgadillo-Hinojosa, G. Cervantes-Díaz, J. R. Lara-Lara, V. Camacho-Ibar, A. Siqueiros-Valencia, and C. Bazán-Guzmán (2010), Temporal variability of the physical and chemical water column characteristic at a coastal monitoring observatory: Station ENSENADA, *Cont. Shelf Res.*, *30*, 1730–1742.

Liss, P. S., and L. Merlivat (1986), Air-sea gas exchange rates: Introduction and synthesis, in *The Role of Air-Sea Exchange in Geochemical Cycling*, edited by P. Buat-Menard, pp. 113–129, Reidel, Boston.

Lueker, T. J., S. J. Walker, M. K. Vollmer, R. F. Keeling, C. D. Nevison, R. F. Weiss, and H. E. Garcia (2003), Coastal upwelling air-sea fluxes revealed in atmospheric observations of O2/N2, CO$_2$ and N2O, *Geophys. Res. Lett.*, *30*, 1292, doi:10.1029/2002GL016615.

Lueger, H., R. Wanninkhof, A. Olsen, J. Triñanes, T. Johannessen, D. W. R. Wallace, and A. Körtzinger (2008), The sea-air CO$_2$ flux in the North Atlantic estimated from satellite and ARGO profiling float data, *NOAA Tech. Memo. OAR AOML-96*, 28 pp., Atlantic Oceanogr. and Meteorol. Lab., NOAA, Miami, Fla.

Martinez-Diaz-De-Leon, A. (2004), Spatial variability of wave data from Todos Santos Bay, Baja California, Mexico, *J. Coast. Res.*, *20*, 1231–1236.

McGillis, W. R., J. B. Edson, J. D. Ware, J. W. H. Dacey, J. E. Hare, C. W. Fairall, and R. Wanninkhof (2001), Carbon dioxide flux techniques performed during GasEx-98, *Mar. Chem.*, *75*, 267–280.

McNeil, B. I., N. Metzl, R. M. Key, R. J. Matear, and A. Corbiere (2007), An empirical estimate of the Southern Ocean air-sea CO$_2$ flux, *Global Biogeochem. Cycles*, *21*, GB3011, doi:10.1029/2007GB002991.

Moffat, A., et al. (2007), Comprehensive comparison of gap-filling technique for eddy covariance net carbon fluxes, *Agric. Forest Meteorol.*, *148*, 821–838.

Moncrieff J., R. Clement, J. Finnigan, T. Meyers (2004), Averaging, detrending, and filtering of Eddy Covariance time series, in *Handbook of Micrometeorology*, edited by. Lee X., Massman W. J., and Law B. E., pp. 7–31, Springer, the Netherlands.

Nightingale, P. D., P. S. Liss, and P. Schlosser (2000), Measurements of air-sea gas transfer during an open ocean algal bloom, *Geophys. Res. Lett.*, *27*, 2117–2120.

Norris, S. J., I. M. Brooks, G. de Leeuw, M. H. Smith, M. Moerman, and J. N. Lingard (2008), Eddy covariance measurements of sea spray particles over the Atlantic Ocean, *Atmos. Chem. Phys.*, *8*, 555–563.

Palacios, D. M., S. J. Bograd, R. Mendelssohn, and F. B. Schwing (2004), Long-term and seasonal trends in stratification in the California Current, 1950–1993, *J. Geophys. Res.*, *109*, C10016, doi:10.1029/2004JC2280.

Pennington, J. T., G. E. Friederich, C. G. Castro, C. A. Collins, W. W. Evans, and F. P. Chavez (2009), A carbon budget for the northern and central California coastal upwelling system, in *Carbon and Nutrient Fluxes in Continental Margins*, edited by Liu K.-K., L. Atkinson, R. Quinones, and L. Talaue-McManus, 740 pp., Springer

Riley, W. J., J. T. Randerson, P. N. Foster, and T. J. Lueker (2005), Influence of terrestrial ecosystems and topography on coastal CO$_2$ measurements: A case study at Trinidad Head, California, *J. Geophys. Res.*, *110*, 1–15, doi:10.1029/2004JG000007.

Ribas-Ribas, M., J. M. Hernández-Ayón, V. F. Camacho-Ibar, A. Cabello-Pasini, A. Mejia-Trejo, R. Durazo, S. Galindo-Bect, A. J. Souza, J. M. Forja, and A. Siqueiros-Valencia (2011), Effects of upwelling, tides and biological processes on the inorganic carbon system of a coastal lagoon in Baja California, *Estuaries Coastal Shelf Sci.*, *95*, 367–376.

Sarmiento, J. L., and N. Gruber (2006), *Ocean Biogeochemical Dynamics*, 464 pp., Princeton University Press, Princeton, N. J.

Schotanus, P., F. T. M. Nieuwstadt, and H. A. R. De Bruin (1983), Temperature measurement with a sonic anemometer and its application to heat and moisture fluxes, *Boundary Layer Meterol.*, *26*, 81–93.

Schuepp, P. H., M. Y. Leclerc, J. I. MacPherson, and R. L. Desjardins (1990), Footprint prediction of scalar fluxes from analytical solutions of the diffusion equation, *Boundary Layer Meterol.*, *50*, 355–373.

Smith, S. V. (1981), Marine macrophytes as a global carbon sink, *Science*, *211*, 838–840.

Smith, S. V., and J. T. Hollibaugh (1993), Coastal metabolism and the oceanic carbon balance, *Rev. Geophys.*, *31*, 75–89.

Takahashi, T., et al. (2002), Global sea-air CO$_2$ flux based on climatological surface ocean pCO$_2$, and seasonal biological and temperature effects, *Deep Sea Res., Part II*, *49*, 1601–1622.

Takahashi, T., et al. (2009), Climatological mean and decadal changes in surface ocean pCO$_2$, and net sea-air CO$_2$ flux over the global oceans, *Deep Sea Res., Part II*, *56*, 554–577.

Takesue, R. K., and A. van Geen (2002), Nearshore circulation during upwelling inferred from the distribution of dissolved cadmium off the Oregon coast, *Limnol. Oceanogr.*, *47*, 176–185.

Thomas, H., Y. Bozec, K. Elkalay, and H. J. de Baar (2004), Enhanced open ocean storage of CO$_2$ from shelf sea pumping, *Science*, *304*, 1005–1008.

Torres, R., D. R. Turner, N. Silva, and J. Rutllant (1999), High short-term variability of CO$_2$ fluxes during an upwelling event off the Chilean coast at 30°S, *Deep Sea Res. Part I*, *46*, 1161–1179, doi:10.1016/S0967-0637(99)00003-5.

Torres, R., D. Turner, J. Rutllant, and N. Lefèvre (2003), Continued CO$_2$ outgassing in an upwelling area off northern Chile during the development phase of El Niño 97–98 (July 1997), *J. Geophys. Res.*, *108*, 3336, doi:10.1029/2000JC000569.

Vandemark, D., J. E. Salisbury, C. W. Hunt, S. M. Shellito, J. D. Irish, W. R. McGillis, C. L. Sabine, and S. M. Maenner (2011), Temporal and spatial dynamics of CO$_2$ air-sea flux in the Gulf of Maine, *J. Geophys. Res.*, *116*, C01012, doi:10.1029/2010JC006408.

Vargas, R., et al. (2010), Looking deeper into the soil: biophysical controls and seasonal lags of soil CO$_2$ production and efflux, *Ecol. Appl.*, *20*, 1569–1582.

Vargas, R., H. W. Loescher, T. Arredondo, E. Huber-Sannwald, R. Lara-Lara, and E. A. Yépez (2012), Opportunities for advancing carbon cycle science in Mexico: Toward a continental scale understanding, *Environ. Sci. Policy*, *21*, 84–93.

Vargas, R., et al. (2013), Progress and opportunities for monitoring greenhouse gases fluxes in Mexican ecosystems: The MexFlux network. *Atmosfera*, *26*, 325–336.

Vickers, D., and L. Mahrt (1997), Quality control and flux sampling problems for tower and aircraft data, *J. Atmos. Oceanic Technol.*, *14*, 512–526.

Wanninkhof, R. (1992), Relationship between wind speed and gas exchange over the ocean, *J. Geophys. Res.*, *97*, 7373–7382.

Wanninkhof, R., and W. McGillis (1999), A cubic relationship between air-sea CO$_2$ exchange and wind speed, *Geophys. Res. Lett.*, *26*, 1889–1892.

Wanninkhof, R., W. E. Asher, D. T. Ho, C. Sweeny, and W. R. McGillis (2009), Advances in quantifying air-sea gas exchange and environmental forcing, *Annu. Rev. Marine Sci.*, *1*, 213–244.

Wollast, R. (1991), The coastal organic carbon cycle: Fluxes, sources, and sinks, in *Ocean Margin Processes in Global Change*, edited by R. F. C. Mantoura, J. M. Martin, and R. Wollast, pp. 365–381, John Wiley and Sons Ltd, Chichester.

Yelland, M. J., R. W. Pascal, P. K. Taylor, and B. I. Moat (2009), Auto-Flux: An autonomous system for the direct measurement of the air-sea fluxes of CO$_2$, heat and momentum, *J. Oper. Ocean.*, *2*, 15–23.

Zhang, X. (2012), Contribution to the global air-sea CO$_2$ exchange budget from asymmetric bubble-mediated gas transfer, *Tellus Ser. B*, *64*, doi:10.3402/tellusb.v64i0.17260.

Zhao, D., Y. Toba, Y. Suzuki, and S. Komori (2003), Effect of wind waves on air-sea gas exchange: Proposal of an overall CO$_2$ transfer velocity formula as a function of breaking-wave parameter, *Tellus*, *55B*, 478–487.